IEEE Access
Multidisciplinary | Rapid Review | Open Access Journal

Received August 7, 2020, accepted August 22, 2020, date of publication August 26, 2020, date of current version September 9, 2020.

Digital Object Identifier 10.1109/ACCESS.2020.3019638

Probabilistic Principal Component Analysis Assisted New Optimal Scale Morphological Top-Hat Filter for the Fault Diagnosis of Rolling Bearing

SIYU ZHAO[1], CHANGZHENG CHEN[1,2], AND YUANQING LUO[1]
[1]School of Mechanical Engineering, Shenyang University of Technology, Shenyang 110870, China
[2]Liaoning Engineering Center for Vibration and Noise Control, Shenyang 110870, China

Corresponding author: Changzheng Chen (czchen@sut.edu.cn)

This work was supported by the National Natural Science Foundation of China under Grant 51675350 and Grant 51705337.

ABSTRACT The early fault impulses of rolling bearing are often submerged by harmonic interferences and background noise. In this paper, a fault diagnosis scheme called probabilistic principal component analysis assisted optimal scale average of erosion and dilation hat filter (OSAEDH-PPCA) is presented for the fault detection of rolling bearing. Based on morphological erosion operator and morphological dilation operator, a new morphological top-hat operator, namely average of erosion and dilation hat (AEDH) operator is firstly proposed to extract the fault impulses in the vibration signal. Simulation analysis shows the filter characteristics of proposed AEDH operator. Comparative analyses demonstrate that the feature extraction property of the AEDH operator is superior to existing top-hat operators. Then, the probabilistic principal component analysis is introduced to enhance the filter property of AEDH for highlighting the fault feature information of rolling bearing further. Experimental signals collected from the test rig and the engineering are employed to validate the availability of proposed method. Experimental results show that the OSAEDH-PPCA can effectively extract the early fault impulses from vibration signal of rolling bearing. Comparison results verify that the OSAEDH-PPCA has advantage in early fault detection of rolling bearing than other morphological filters in existence.

INDEX TERMS Rolling bearing, morphological filter, morphological operator, probabilistic principal component analysis, fault diagnosis.

NOMENCLATURE

Acronyms

MM	mathematical morphology
MF	morphological filter
AVG	average of opening and closing
CMF	average of opening-closing and closing-opening
MG	gradient of dilation and erosion
DIF	gradient of opening and closing
AVGH	average of opening and closing hat
CMFH	average of opening-closing and closing-opening hat
SE	structure element
WTH	white top-hat
AED	average of erosion and dilation
AEDH	average of erosion and dilation hat
OSAEDH	optimal scale average of erosion and dilation hat filter
PPCA	probabilistic principal component analysis
CC	correlation coefficient
FEF	feature energy factor
SNR	signal-to-noise ratio
AMCMFH	adaptive multiscale CMFH transform
AMAVGH	adaptive multiscale AVGH transform
$AMMG_{DE}$	averaged multiscale MG filter
$AMMG_{CO}$	averaged multiscale DIF filter
ACDIF	average combination difference morphological filter

The associate editor coordinating the review of this manuscript and approving it for publication was Ruqiang Yan.

I. INTRODUCTION

As an important part of rotating machinery, the failure of rolling bearings is one of the common causes of mechanical

fault [1], [2]. When a rolling bearing has local defects, periodic impulses will be generated during the rotation. Hence, timely detection of those impulses can reduce the loss caused by failure. However, the fault impulses in the vibration signal are always overwhelmed by a large amount of background noise and complex interferences. Therefore, an effective fault feature extraction method may be very important for fault diagnosis of rolling bearings [3], [4].

Recently, many signal processing methods have been successfully applied to fault diagnosis of the rolling bearings, such as WT [5], SK [6], EMD [7], VMD [8], etc. However, these signal analysis methods have their own shortcomings. WT analysis needs to select a suitable wavelet basis in advance, which may lead to limitations for application [9]. The feature extraction capability of SK method will be affected by the noise in vibration signal [10]. As a recursive decomposition method, EMD may encounter the end effects, mode mixing, overshoot and undershoot problems during signal processing [11]. Compared with EMD, VMD may be more suitable for the feature extraction of vibration signals [12]. When the VMD method is selected for fault diagnosis, two important parameters (the decomposed modes K and the balance parameter α) need to be given in advance. Unfortunately, how to determine the two parameters lack of the corresponding theoretical support [13].

Different from traditional fault diagnosis methods, mathematical morphology (MM) is a novel signal processing method for extracting the fault information of rolling bearing [14], [15]. Originally, MM is introduced into image processing by Serra [16] as an image analysis method. In recent years, some scholars have gradually applied MM to one-dimensional signal processing. When MM is applied to signal processing, it is often called morphological filter (MF). In the basic theory of MF, feature extraction and noise reduction are achieved by morphological operation of structure element and original signal. The performance of MF mainly depends on two important parameters, namely morphological operator and structure element [17].

There are four basic morphological operators in the morphological filter, including dilation, erosion, opening and closing [18]. In order to filter the noise or extract the feature, some scholars proposed a series of cascade operators based on four basic operators. Dong *et al.* [19] proposed the average of opening and closing (AVG) operator and validated its capability of high level noise suppression. Wang *et al.* [20] and Costa *et al.* [21] adopted the average of opening-closing and closing-opening operator (CMF) to extract impulses and filter noise. However, Hu *et al.* [22] showed that the average operators could be regarded as a kind of low pass filter, which was not good enough in feature extraction. In order to extract the features in the signal, Li *et al.* [23] and Raj A *et al.* [24] proposed the gradient of dilation and erosion (MG) operator. Li *et al.* [25] and Zhang *et al.* [26] successfully detected the local defect of the rolling bearing by using the gradient of opening and closing (DIF) operator. Although the gradient operators could extract the fault information in the signal, some details of the information would be lost [27]. In order to extract more fault feature information, some scholars proposed morphological top-hat operators. Yan *et al.* [28] employed average of opening and closing hat (AVGH) operator to extract fault impulses from the vibration signal of rolling bearing. After analyzing the characteristics of CMF operator, Hu *et al.* [22] proposed the CMF-hat (CMFH) operator and applied it in fault diagnosis of rolling bearing. However, these morphological top-hat operators based on the opening and closing operator still have the deficiency of losing the fault information.

Structure element (SE) has two important attributes, including shape and scale. For different signals, scholars have designed some SEs with different shapes and applied them to the fault diagnosis of rolling bearings [20], [29]–[31]. However, most scholars have shown that the shape of SE has little influence on the filter property of MF [19], [27], [32], [33]. In addition, the scale of SE has a great influence on the filtered results [23]. In order to obtain the optimal filtered result, single scale MF [19], [34], [35] and multiscale MF [29], [36] have been proposed by some scholars. Nevertheless, the fault information distributed in other SE scales will not be extracted by the single scale MF [37]. Multiscale MF can extract fault information distributed in different SE scales. Unfortunately, too large or too small SE scales will bring the interferences into the filtered result [25]. The existence of these interferences will affect the filter property of multiscale MF instead. Therefore, the selection of reasonable SE scale is still a hot topic in the study of MFs.

In view of the fault impulses are often overwhelmed by noise and interferences, the probabilistic principal component analysis assisted optimal scale average of erosion and dilation hat filter (OSAEDH-PPCA) is proposed for the fault detection of rolling bearing. Firstly, a new morphological top-hat operator called average of erosion and dilation hat (AEDH) is proposed according to basic erosion and dilation operator. Different simulation results show that the feature extraction capability of AEDH operator is better than the existing top-hat operators. In the next, an enhancement method is adopted for further improving the filtered performance of AEDH.

Considering that the morphological top-hat operators are interfered by noise inevitably, which will affect the filter property of AEDH. When the fault impulses in vibration signal are very weak, traditional de-noising method may filter the fault information by mistake. Different from traditional noise reduction method, probabilistic principal component analysis (PPCA) can decompose the feature information and the noise information into unrelated components [38]. In the PPCA model, it can assume that the feature information and the noise information exist in the orthogonal components respectively [39]. Then, the decomposed components can be obtained by iterating the PPCA model through the expectation maximization algorithm [40]. Finally, comparing the eigenvalues of the covariance matrix, the principal feature component mainly containing fault information can be obtained, while other orthogonal components mainly

contain noise. Through the PPCA analysis, feature information and noise will be stored in different components. Therefore, by employing PPCA to enhance the filter capability of AEDH, the OSAEDH-PPCA can be obtained to highlight the fault information in vibration signal.

In the following, Section 2 introduces the basic theory of mathematical morphology and proposes the AEDH operator. Section 3 studies the filter property of AEDH operator and compares the feature extraction ability of AEDH with other morphological top-hat operators. Section 4 proposes the OSAEDH-PPCA based on AEDH and PPCA, and the extraction performance of OSAEDH-PPCA is demonstrated by a simulated signal. Section 5 verifies the proposed OSAEDH-PPCA by two experimental signals. Section 6 are the conclusions of this paper.

II. THEORIES OF THE MORPHOLOGICAL FILTERS

A. MORPHOLOGICAL OPERATOR

In fact, the fault detection mechanism of MF is to employ morphological operations between the original signal and the structure element. In the morphological filter, different kinds of morphological operations can be collectively called morphological operators. Therefore, a brief review of the existing morphological operators is introduced in the following part.

Assuming that the original signal $f(n)$ is a group of one-dimensional discrete array $F(0, 1, 2, \ldots, N-1)$. The structure element $g(m)$ is defined as another one-dimensional discrete array $G(0, 1, 2, \ldots, M-1)$ and satisfies $N \geq M$. Then, four basic morphological operators can be expressed as:

Dilation:

$$(f \oplus g)(n) = \max[f(n-m) + g(m)] \tag{1}$$

Erosion:

$$(f \Theta g)(n) = \min[f(n+m) - g(m)] \tag{2}$$

Opening:

$$(f \circ g)(n) = (f \Theta g \oplus g)(n) \tag{3}$$

Closing:

$$(f \cdot g)(n) = (f \oplus g \Theta g)(n) \tag{4}$$

where $\oplus$, Θ, $\circ$, $\cdot$ represent the dilation, erosion, opening and closing operation, respectively. Next, the closing-opening operator and the opening-closing operator can be given as:

Opening-closing:

$$F_{OC}(f(n)) = (f \circ g \cdot g)(n) \tag{5}$$

Closing-opening:

$$F_{CO}(f(n)) = (f \cdot g \circ g)(n) \tag{6}$$

Two basic morphological top-hat operators, namely white top-hat (WTH) and black top-hat (BTH), can be represented by Eq. (7) and Eq. (8) respectively. Both the WTH operator and the BTH operator can extract the impulses in the vibration signal.

White top-hat (WTH):

$$WTH(f(n)) = f(n) - (f \circ g)(n) \tag{7}$$

Black top-hat (BTH):

$$BTH(f(n)) = (f \cdot g)(n) - f(n) \tag{8}$$

Morphological gradient operator [36] and morphological difference operator [32] can be defined as:

Morphological gradient operator (MG):

$$MG(f(n)) = (f \oplus g)(n) - (f \Theta g)(n) \tag{9}$$

Morphological difference operator (DIF):

$$DIF(f(n)) = (f \cdot g)(n) - (f \circ g)(n) \tag{10}$$

Moreover, the AVG [19] and the AVGH [28] operator can be expressed as:

Average of opening and closing (AVG):

$$AVG(f(n)) = \frac{(f \circ g)(n) + (f \cdot g)(n)}{2} \tag{11}$$

Average of opening and closing hat (AVGH):

$$AVGH(f(n)) = f(n) - \frac{(f \circ g)(n) + (f \cdot g)(n)}{2} \tag{12}$$

Furthermore, the CMF [20] and the CMFH [22] operator can be given as:

Average of opening-closing and closing-opening (CMF):

$$CMF(f(n)) = \frac{F_{CO}(f(n)) + F_{OC}(f(n))}{2} \tag{13}$$

Average of opening-closing and closing-opening hat (CMFH):

$$CMFH(f(n)) = f(n) - \frac{F_{CO}(f(n)) + F_{OC}(f(n))}{2} \tag{14}$$

B. STRUCTURE ELEMENT

When a morphological operator is determined in the morphological filter, the next step is to select an appropriate structure element. There are different shapes of structure element, such as flat, triangle and semicircle, etc. Many scholars have shown that there is no obvious difference between the flat SE and other shapes of SE in the fault feature extraction. In addition, complex SE shapes will increase the computational load and reduce the computational efficiency. Therefore, the flat SE is adopted in the following research of this paper.

For the flat SE, the relationship between the scale ε and the length L is $L = \varepsilon + 2$. Previous studies have shown that the maximum length of the SE ($L_{\max}$) can be determined as $\lfloor f_s / f_0 \rfloor$ (f_s is the sample frequency, f_0 is the fault frequency, and $\lfloor \cdot \rfloor$ represents the rounding operation) to cover most of the fault information [27], [41].

C. AVERAGE OF EROSION AND DILATION HAT OPERATOR

For the four basic morphological operators, the erosion operator can smooth the valleys of the signal and reduce the peaks of the signal, while the dilation operator can smooth the peaks and improve the valleys [35]. Meanwhile, the closing operator can retain the peaks and remove the valleys in signal, while the opening operator has the opposite effect on signals as the closing operator. Previous study has shown that a single morphological operator can only extract the unidirectional impulses in signal [19]. However, the fault signal of rolling bearing is usually regard as bidirectional periodic impulses. Therefore, in Dong's [19] study, the opening and closing operators were employed to propose the AVG operator (Eq. (11)) for removing the harmonic interferences and noise in signal. Furthermore, Yu's [35] study showed that the four basic morphological operators can be divided into two categories. That is to say, dilation and closing operators had similar filter characteristics, while erosion and opening operators had similar filter characteristics. Hence, inspired by previous studies [19], [35], the erosion and dilation operators are applied to propose a new average operator called average of erosion and dilation (AED) for the vibration signal processing of rolling bearings. AED operator can be defined as Eq. (15).

Average of erosion and dilation (AED):

$$AED(f(n)) = \frac{(f\Theta g)(n) + (f \oplus g)(n)}{2} \tag{15}$$

Then, Hu's [22] study indicated that the average operators such as AVG (Eq. (11)) and CMF (Eq. (13)) can be regarded as a low-pass filter. Furthermore, the low-pass filter was inadequate in fault feature extraction. On the contrary, morphological top-hat operators could be regarded as a high-pass filter. Therefore, combined the characteristics of top-hat operators and average operators, Hu [22] proposed the CMFH operator (Eq. (14)) for extracting the fault features. Similarly, a new combined morphological top-hat operator, namely average of erosion and dilation hat (AEDH), can be proposed to extract the fault impulses in vibration signal. AEDH operator can be expressed as:

Average of erosion and dilation hat (AEDH):

$$AEDH(f(n)) = f(n) - \frac{(f\Theta g)(n) + (f \oplus g)(n)}{2} \tag{16}$$

III. PROPERTY OF THE AEDH OPERATOR

In this section, the property of AEDH operator is demonstrated by introducing a series of simulation analyses. Because the MF does not have a definite transfer function, it is difficult to directly derive its filter characteristics. However, the frequency response characteristics of MF can be approximately demonstrated by the amplitude response of sinusoidal excitation input signal. The sinusoidal excitation input signal can be defined in Eq. (17).

$$\begin{cases} k(n) = \sin(2\pi f \cdot \dfrac{m}{f_s} + 2\pi \dfrac{f}{f_s} \cdot \dfrac{i}{10}) \\ \quad m = 0, 1, \ldots, M-1 \\ \quad i = 0, 1, \ldots, 9 \\ f = \dfrac{f_s}{M}, \dfrac{2f_s}{M}, \dfrac{3f_s}{M}, \ldots, (\dfrac{M}{2} - 1)\dfrac{f_s}{M} \end{cases} \tag{17}$$

where f_s is the sampling frequency, and M is the sampling number. More details of Eq. (17) are shown in [22]. By changing the frequency f of the sinusoidal excitation signal, the frequency response of the AEDH at different frequencies can be obtained. In the following, the influences of SE scale ε and sampling frequency f_s on the frequency response characteristics of AEDH are studied.

Fig. 1 shows the amplitude response of AEDH operator when the f changes. According to the frequency response characteristics, the AEDH operator can be regarded as a high pass filter. In Fig. 1(a), set $f_s = 1$ Hz, $M = 1024$. It can be concluded that the change of SE scale will have effect on the filter characteristics of AEDH operator. With the increase of SE scale, the cutoff frequency of AEDH will decrease and the passband range will become larger. Within the passband of the filter, the amplitude response fluctuation will decrease as the SE scale increases. In addition, the transition band of the filter will become steeper with the increase of SE scale. In Fig. 1(b), set $\varepsilon = 8$, $M = 1024$. It can be obtained that a higher sampling frequency will correspond to a higher cutoff frequency and the transition band will be more gentle.

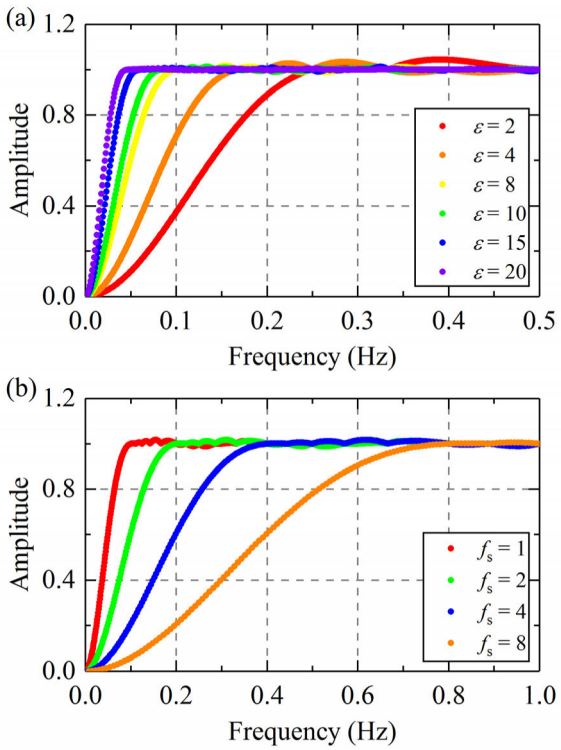

FIGURE 1. Frequency response of the AEDH operator.

Since the principle of MF is to extract the feature information by changing the shape of the signal, the property of AEDH operator cannot be fully demonstrated through the frequency response characteristics. Hence, in order to make the research close to the application of rolling bearing fault diagnosis, a simulation signal is established to assess the extraction performance of AEDH operator. When local defects occur in the rolling bearing, it can generate a series of low frequency impulses. Moreover, the low frequency impulses will excite the inherent vibration near the defect site. That is to say, the fault signal of the rolling bearing can be represented as an impulse modulated signal [25]. In modulated signal, the carrier frequency is the inherent frequency near the defect site, and the modulation frequency is the bearing fault frequency. Furthermore, in the signal collected from real site, the fault impulses are often submerged by harmonics and noise. Therefore, according to [25], a simulation signal including harmonics can be expressed as:

$$x(t) = x_1(t) + x_2(t) \tag{18}$$

where simulated fault impulses $x_1(t)$ can be defined by $4{\cdot}\exp(-\omega \cdot t){\cdot}\sin(2\pi \cdot f_n \cdot t)$. $\omega = 100$ is the decay parameter of exponential decaying impulsive signal, and $f_n = 200$ represents the inherent frequency. The periodical frequency f_0 of simulated fault impulses is 16 Hz. $x_2(t) = 1.2 \cdot \sin(2\pi \cdot f_1 \cdot t) + 1.1 \cdot \cos(2\pi \cdot f_2 \cdot t)$ ($f_1 = 30$ Hz, $f_2 = 40$ Hz) represents the harmonic interferences in the signal. The sampling frequency is 1024 Hz and the length of signal is 1024.

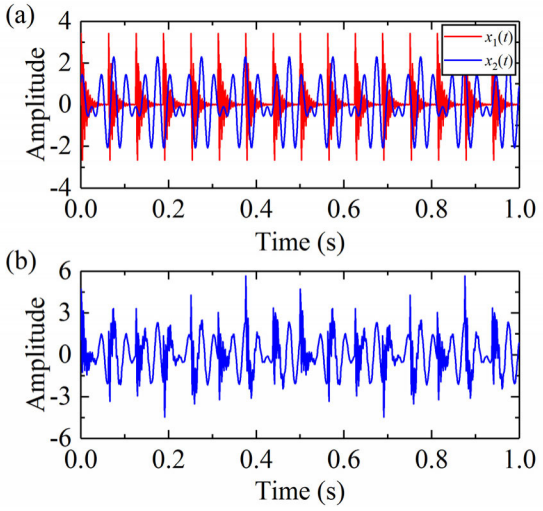

FIGURE 2. Time domain waveforms: (a) $x_1(t)$ and $x_2(t)$, (b) $x(t)$.

Fig. 2 shows the time domain waveforms of the $x_1(t)$, $x_2(t)$, and $x(t)$. It can be concluded that the simulated impulses $x_1(t)$ cannot be observed in Fig. 2(b) clearly because of the influence of $x_2(t)$. In order to extract the simulated impulses, AEDH is employed to process the $x(t)$. For comparison, three existing morphological top-hat operators (WTH, AVGH, and CMFH) are also employed to process the $x(t)$. The analysis results of four operators are shown in Fig. 3. Meanwhile,

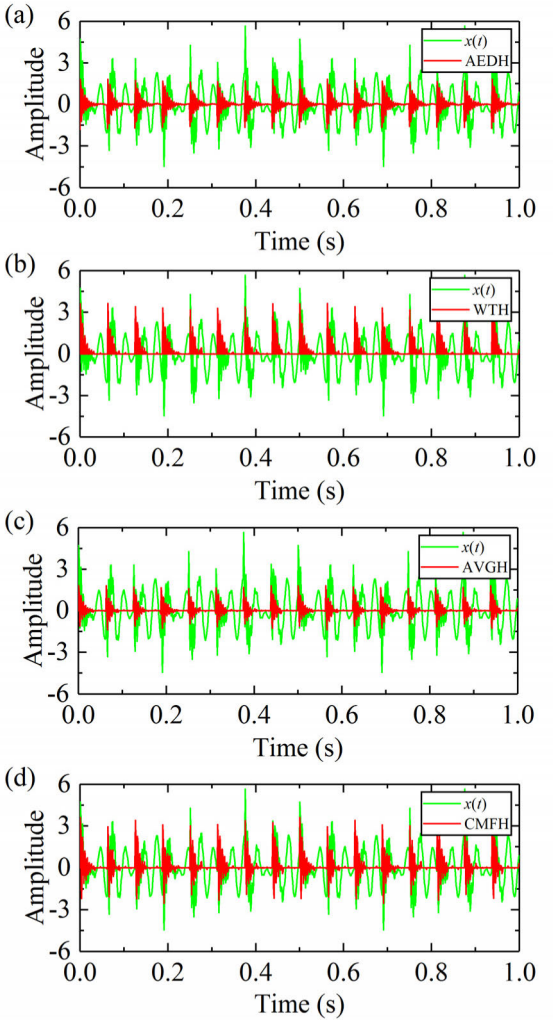

FIGURE 3. Analysis results of different top-hat operators.

in order to quantitative compare the extraction capability of four operators under the same circumstances, the correlation coefficient (CC) is introduced for analyzing the similarity between the filtered results and simulated impulses $x_1(t)$. The correlation coefficient (CC) [42] can be expressed in Eq. (19):

$$CC = \frac{E[(y_1 - \bar{y}_1)(y_2 - \bar{y}_2)]}{\sqrt{E[(y_1 - \bar{y}_1)^2]E[(y_2 - \bar{y}_2)^2]}} \tag{19}$$

where $E[\bullet]$ represents the mathematical expectation, and y_1, y_2 represent two sets of signals. According to [33], CC meets $|CC| \leq 1$. In addition, if the $|CC|$ is larger, the two sets of signals y_1 and y_2 will be more similar. Therefore, a larger CC between the filtered result and $x_1(t)$ means the morphological top-hat operator can extract more simulated fault impulses. The CCs between the filtered results of four operators and simulated impulses $x_1(t)$ are shown in Table 1.

According to Fig. 3(a)-(d), all the four top-hat operators can extract the periodic impulses in signal $x(t)$. However, when the WTH (Fig. 3(b)) is adopted, it is obvious that the negative peaks in the filtered result are completely eliminated.

TABLE 1. The *CC*s of different morphological top-hat operators.

Morphological top-hat operators	Correlation coefficient (*CC*)
AEDH	0.93
AVGH	0.90
CMFH	0.87
WTH	0.74
$x_1(t)$	1.00

According to the discussions in Section 2.3, the reason for this phenomenon is that only a single morphological operator (opening) is adopted in WTH. Additionally, the *CC* of WTH (0.74) is the lowest among four operators. AEDH (Fig. 3(a)), AVGH (Fig. 3(c)) and CMFH (Fig. 3(d)) can suppress the harmonic interferences and extract the bidirectional peaks in the signal. Nevertheless, the *CC*s of AVGH (0.90) and CMFH (0.87) are less than AEDH (0.93), which means part of the feature information is filtered out wrongly. In the application of fault diagnosis, using AVGH or CMFH may lose some fault features, which will affect the feature extraction capability of MF. Compared with other top-hat operators, AEDH obtains the largest *CC* among the four operators. It means that using AEDH operator can extract the fault impulses more completely. Therefore, AEDH has obvious advantages over other morphological top-hat operators in the extraction of feature information.

In practical application, the vibration signal of rolling bearing contains not only harmonic interferences, but also much noise. The noise will have effect on the fault detection of rolling bearing. For further discussing the property of AEDH operator, the gauss white noise $\delta(t)$ is added to the simulation signal $x(t)$. Another simulation signal $y(t)$ composed of $x(t)$ and $\delta(t)$ can be defined as:

$$y(t) = x(t) + \delta(t) = x_1(t) + x_2(t) + \delta(t) \tag{20}$$

Meanwhile, an evaluation indicator called feature energy factor (FEF) [43] is adopted to evaluate the feature extraction capability of the above four top-hat operators. The FEF can be expressed in Eq. (21):

$$FEF = \frac{\sum_{i=1}^{m} Y^2(i)}{\sum Y^2} \tag{21}$$

where $Y(i)$ represents the amplitude of fault frequency and its harmonics. The m is selected as 5. Y represents the amplitude of all frequency components in the envelope spectrum. The definition of FEF denotes the energy ratio of fault information in the envelope spectrum. When the FEF value of the signal is large, it will be more fault information in the signal.

Then, when the signal-to-noise ratio (SNR) of $y(t)$ changes from -10 to 0, AEDH, AVGH, CMFH, and WTH operator are adopted to process the different simulation signals $y(t)$. At the same time, FEF values of the filtered results under different SNR can be calculated. Fig. 4 shows the FEF curves of

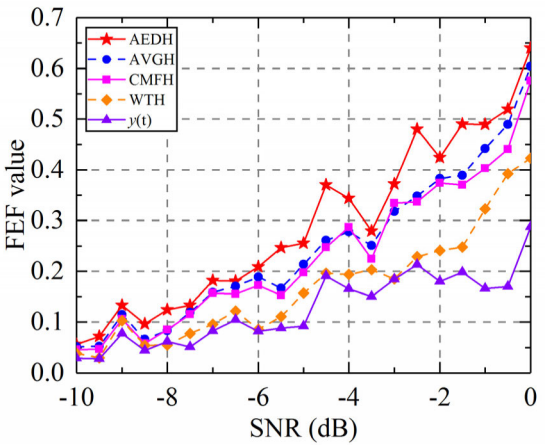

FIGURE 4. FEF curve of different top-hat operators.

the analysis results, when the SNR of $y(t)$ changes. In Fig. 4, the feature extraction capability of proposed AEDH operator is superior to other morphological top-hat operators under different SNR conditions. When there is high level noise in the simulation signal $y(t)$, it is obvious that AEDH operator can extract more simulated impulses than other top-hat operators. When $y(t)$ mainly contains noise, the feature extraction capability of AEDH will be weaken, but it is still better than other top-hat operators. When the noise in the signal is weak, all the four top-hat operators can effectively extract the simulated impulses. Meanwhile, the AEDH operator is still superior to other top-hat operators. The extraction capability of AVGH and CMFH is similar when there is high level noise in the signal. Moreover, when the noise level in the signal gradually decreased, the AVGH operator performed slightly better than the CMFH operator. Furthermore, there is no obvious difference between the filtered result of WTH and the original signal $y(t)$ under low SNR. That indicates the WTH cannot effectively detect the fault when there is high level noise in the signal. Therefore, the comparison studies further verify the superiority of AEDH operator in fault feature extraction.

IV. THE PROPOSED OSAEDH-PPCA

A. BRIEF INTRODUCTION OF PPCA

According to the discussion in Section 3, when the SNR increases, the extraction capability of AEDH operator will decrease. This phenomenon is mainly caused by the theory of the morphological top-hat operation. The original signal participates in the morphological top-hat operation for retaining the details of feature information. However, if the original signal contains overmuch noise, the extraction capability of the top-hat operators will be weakened. Therefore, in order to extract the fault feature information of rolling bearing under high level noise, probabilistic principal component analysis is introduced to enhance the extraction performance of AEDH operator. In the following, the principle of the probabilistic

principal component analysis in one-dimensional signal is reviewed briefly.

Probabilistic principal component analysis (PPCA) can decompose high-dimensional data into some unrelated low-dimensional data [38]. Based on the principle of PPCA, an appropriate probability model will be firstly built for each variable. Then, through orthogonal projection of the original variable data on the principal component matrix, the decomposed components can be obtained. The principal feature component is usually determined by the direction with the largest variance. For the feature extraction, it can be assumed that the fault feature information mainly exists in the principal feature component and noise information exists in the orthogonal direction of the principal feature component [39]. After PPCA analysis, the fault information and the noise information will store in unrelated components respectively, which can remove the noise in the signal [44].

Assuming that the filtered result of AEDH is $y(N)$ ($N = 1, 2, 3, \ldots, N$). In order to separate the fault information component and noise component, $y(N)$ can be constructed as a n-dimensional Hankel matrix $\mathbf{X}$ [45].

$$\mathbf{X} = \begin{bmatrix} y(1) & y(2) & \ldots & y(m) \\ y(2) & y(3) & \ldots & y(m+1) \\ \ldots & \ldots & \ldots & \ldots \\ y(n) & y(n+1) & \ldots & y(N) \end{bmatrix} \tag{22}$$

where $m = N\text{-}n + 1$. In the principle of PPCA, it assumes that the n-dimensional variable data $\mathbf{X}$ can be composed of the following model.

$$\mathbf{X} = \mathbf{P} \cdot \mathbf{u} + \mathbf{E} + \mu \tag{23}$$

where $\mathbf{X} = \{\mathbf{x}_1, \mathbf{x}_2, \cdots \mathbf{x}_m\} \in \mathbf{R}^{n\times m}$ is the Hankel matrix composed of the filtered result of AEDH. $\mathbf{P} = \{\mathbf{p}_1, \mathbf{p}_2, \cdots \mathbf{p}_m\} \in \mathbf{R}^{n\times k}$ represents the linear transformation (principal component matrix) from the latent variable space to the original variable space and satisfies $k < n$. $\mathbf{u} = \{\mathbf{u}_1, \mathbf{u}_2, \cdots \mathbf{u}_m\} \in \mathbf{R}^{k\times m}$ represents m-dimensional gauss latent variable. $\mathbf{E}$ is the zero mean gauss noise matrix. $\mathbf{u}$ and $\mathbf{E}$ satisfy $\mathbf{u} \sim N(0, \mathbf{I})$, $\mathbf{E} \sim N(0, \sigma^2\mathbf{I})$. $\mathbf{I}$ and σ^2 represent the unit matrix and the variance of the noise respectively. The μ is the mean value of original variable $\mathbf{X}$. In order to simplify the calculation, Eq. (24) can be obtained by mean-subtraction of the original variable $\mathbf{X}$.

$$\mathbf{X} = \mathbf{P} \cdot \mathbf{u} + \mathbf{E} \tag{24}$$

According to PPCA's assumption, $\mathbf{X}$ obeys the following gauss distribution:

$$\mathbf{X} \sim N(0, \mathbf{P}\mathbf{P}^T + \sigma^2\mathbf{I}) \tag{25}$$

Meanwhile, the probability distribution of the latent variable $\mathbf{u}$ can be defined as:

$$p(\mathbf{u}) = (2\pi)^{-k/2} e^{(-\frac{1}{2\sigma^2}\mathbf{X}^T\mathbf{X})} \tag{26}$$

Since $\mathbf{X}$ is composed by the latent variable $\mathbf{u}$, the probability distribution of $\mathbf{X}$ under the condition of $\mathbf{u}$ is $p(\mathbf{X}|\mathbf{u})$. The $p(\mathbf{X}|\mathbf{u})$ can be expressed as:

$$p(\mathbf{x}|\,\mathbf{u}) = (2\pi)^{-n/2} e^{(-\frac{1}{2\sigma^2}\|\mathbf{X}-\mathbf{P}\cdot\mathbf{u}\|^2)} \tag{27}$$

According to Eq. (26) and Eq. (27), the probability distribution of $\mathbf{X}$ can be expressed as:

$$\begin{cases} p(\mathbf{x}) = \int p(\mathbf{x}|\,\mathbf{u})p(\mathbf{u})d\mathbf{x} \\ \qquad = (2\pi)^{-n/2}\,|\mathbf{C}|^{-1/2}\, e^{(-\frac{1}{2}\mathbf{X}^T\mathbf{C}^{-1}\mathbf{X})} \\ \mathbf{C} = \mathbf{P}\mathbf{P}^T + \sigma^2\mathbf{I} \end{cases} \tag{28}$$

where $\mathbf{C}$ is the covariance matrix determined by $\mathbf{P}$ and σ^2. The estimation values of $\mathbf{P}$ and σ^2 ($\tilde{\mathbf{P}}$ and $\tilde{\sigma}^2$) can be calculated by utilizing the EM algorithm. The $\tilde{\mathbf{P}}$ and $\tilde{\sigma}^2$ can be given as:

$$\begin{cases} \tilde{\mathbf{P}} = \mathbf{S}\mathbf{P}(\sigma^2\mathbf{I} + \mathbf{M}^{-1}\mathbf{P}^T\mathbf{S}\mathbf{P})^{-1} \\ \tilde{\sigma}^2 = \dfrac{1}{n} tr(\mathbf{S} - \mathbf{S}\mathbf{P}\mathbf{M}^{-1}\tilde{\mathbf{P}}^T) \\ \mathbf{S} = \dfrac{1}{m}\sum_{i=1}^{m} \mathbf{x}_i\mathbf{x}_i^T \end{cases} \tag{29}$$

where $\mathbf{S}$ is the covariance matrix of $\mathbf{X}$, $tr(\cdot)$ is the trace of the matrix. When the iteration converges, the estimation values of $\mathbf{P}$ and σ^2 can be obtained. Finally, a complete PPCA model can be established.

In the output of PPCA, the principal feature component (fault feature information) is stored in the direction with the largest variance (the maximum eigenvalue of $\mathbf{S}$ matrix), and its orthogonal directions mainly contain noise. Hence, the filtered results of PPCA assisted AEDH can be obtained by Eq. (30).

$$V = \mathbf{p}_j^T\mathbf{X} \tag{30}$$

where $\mathbf{p}_j$ is one of the column vectors in the principal component matrix $\mathbf{P}$, and that column vector corresponds to the maximum eigenvalue of the $\mathbf{S}$ matrix. In summary, through employing the PPCA to process the filtered results of AEDH at different SE scales, an enhanced AEDH analysis can be obtained, and the fault feature information can be further highlighted.

B. PROCEDURES OF THE PROPOSED OSAEDH-PPCA METHOD

Combining the advantages of AEDH and PPCA, the OSAEDH-PPCA is proposed for the early fault detection of rolling bearings. The flowchart of OSAEDH-PPCA method is shown in Fig. 5. The detailed process of OSAEDH-PPCA mainly include the following parts:

(1) Collect the early fault vibration signal of rolling bearing.

(2) The flat SE is selected in this paper. The maximum length of SE is $\lfloor f_s / f_0 \rfloor$. The original signal is filtered by the AEDH operator, and the results at different SE scales are obtained.

(3) Construct the variable $\mathbf{X}$ at different SE scales based on the filtered results of AEDH. Then, PPCA is applied to $\mathbf{X}$, and

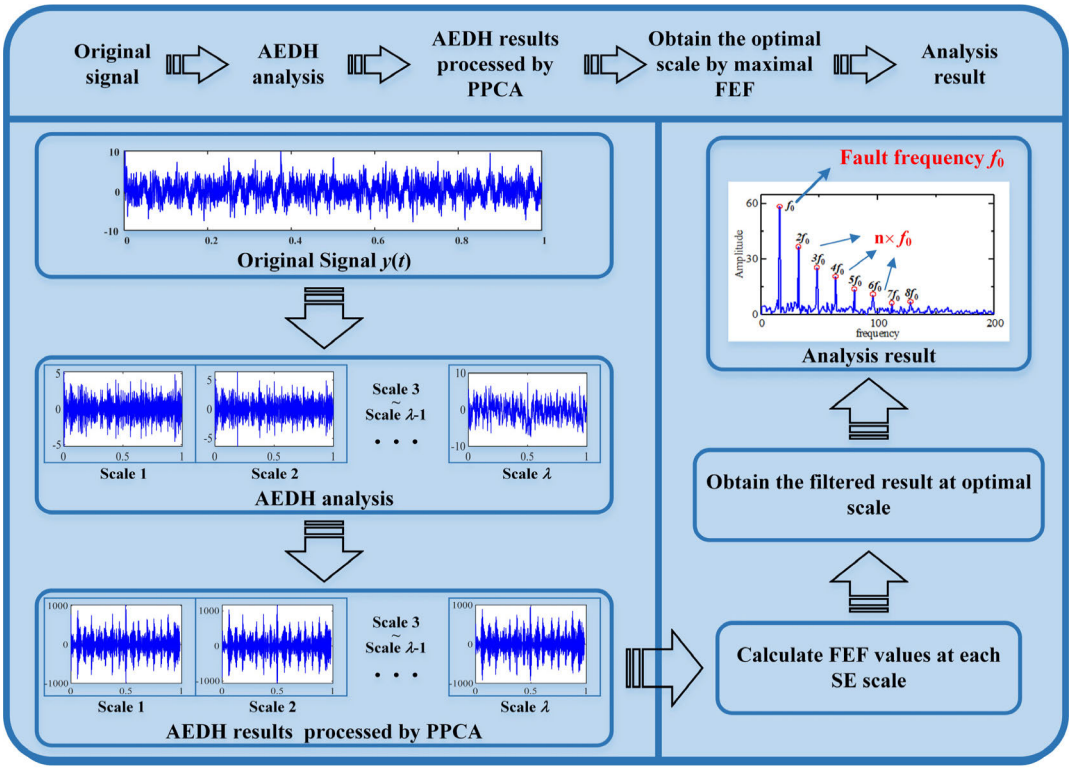

FIGURE 5. Flowchart of the proposed OSAEDH-PPCA.

the filtered results of the AEDH-PPCA at different SE scales are obtained.

(4) Calculate FEF values of the AEDH-PPCA results at different SE scales.

(5) Select the SE scale corresponding to the largest FEF value as the optimal SE scale. The final output is the filtered result of the AEDH-PPCA at optimal scale.

(6) Detect the bearing fault based on the envelope spectrum of the final output.

C. SIMULATED STUDY

In order to demonstrate the performance of the proposed OSAEDH-PPCA clearly, a simulated signal (SNR $= -5$) based on Eq. (20) is introduced for analysis. The simulated signal is shown in Fig. 6.

It can be observed from the envelope spectrum that the simulated fault frequency f_0 cannot be detected, and the dominant peak is 10 Hz (f_2 - f_1). Meanwhile, there is a lot of noise exists in the envelope spectrum. Then, AEDH, PPCA, and OSAEDH-PPCA are used to process the simulated signal respectively. Figs. 7-9 show the filtered results of AEDH, PPCA, and OSAEDH-PPCA.

It can be observed from the envelope spectrum that the simulated fault frequency f_0 cannot be detected, and the dominant peak is 10 Hz (f_2 - f_1). Meanwhile, there is a lot of noise exists in the envelope spectrum. Then, AEDH, PPCA, and OSAEDH-PPCA are used to process the simulated signal

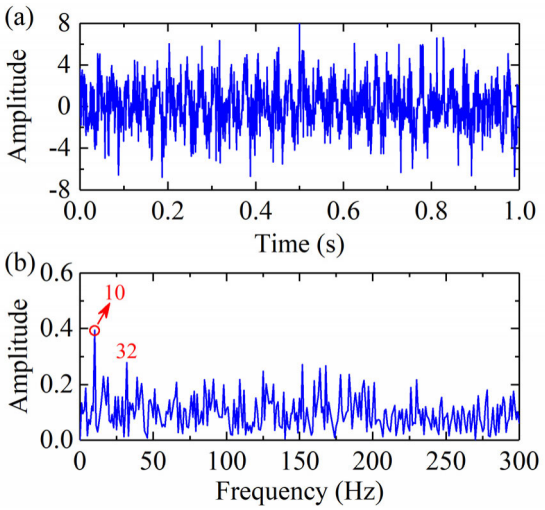

FIGURE 6. Simulated fault signal: (a) time domain waveform, (b) envelope spectrum.

respectively. Figs. 7-9 show the filtered results of AEDH, PPCA, and OSAEDH-PPCA.

In the AEDH analysis, the scale with maximum FEF value is selected as the optimal scale (scale 5, FEF $= 0.26$). According to Fig. 7(b), AEDH operator can extract the fault frequency f_0 and its harmonics ($2f_0$, $3f_0$, $4f_0$, $5f_0$) effectively, and suppresses the interference frequency 10 Hz. However,

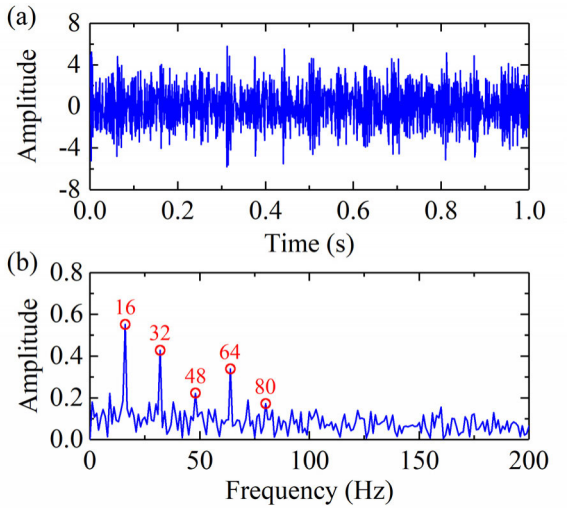

FIGURE 7. The simulated result of AEDH: (a) time domain waveform, (b) envelope spectrum.

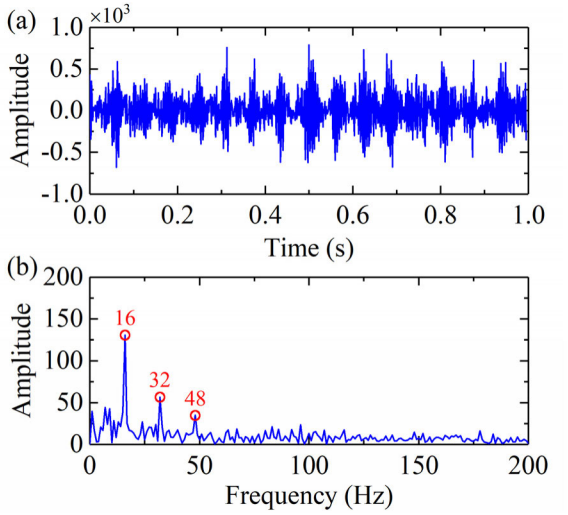

FIGURE 8. The simulated result of PPCA: (a) time domain waveform, (b) envelope spectrum.

some noise is still existing in the envelope spectrum. In Fig. 8, PPCA shows excellent noise reduction ability. It can be observed that most noise is filtered out in the envelope spectrum. Unfortunately, due to excessive noise in the original signal, some fault information is also filtered by PPCA. Hence, compared to Fig. 7(b), PPCA is distinctly inferior to AEDH in the capability of extracting the fault impulses. In the proposed OSAEDH-PPCA, after employing PPCA to further process the AEDH results under different scales, the scale corresponding to the maximum FEF value is selected as the final output (scale 5, FEF = 0.44). Then, in the filtered result of OSAEDH-PPCA (Fig. 9), f_0 and its harmonics ($2f_0 \sim 6f_0$) can be detected clearly in the envelope spectrum. In addition, the noise in the original signal is also effectively suppressed. By comparing the filtered results shown in Figs. 7-9, it can

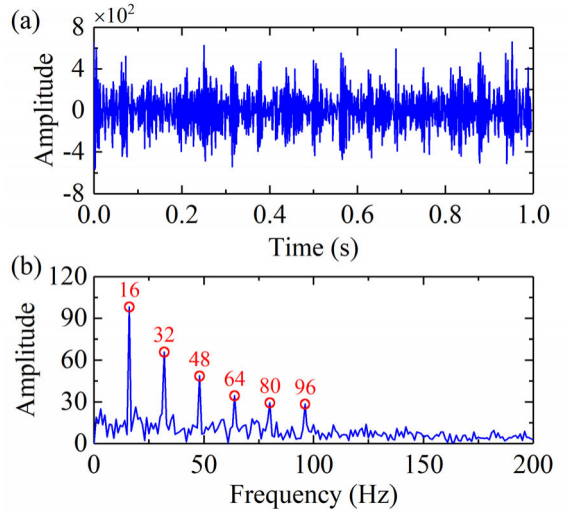

FIGURE 9. The simulated result of proposed OSAEDH-PPCA: (a) time domain waveform, (b) envelope spectrum.

be concluded that the proposed OSAEDH-PPCA has both superior feature extraction capability and noise reduction capability. It means that OSAEDH-PPCA can combine the advantages of AEDH and PPCA and circumvent their respective deficiencies. Therefore, simulated results show that the proposed OSAEDH-PPCA has excellent ability in detecting the fault impulses.

V. APPLICATIONS IN THE FAULT DIAGNOSIS OF ROLLING BEARING

In this section, the effectiveness of proposed OSAEDH-PPCA is verified by the experiment of rolling bearing and the engineering application in wind turbine. In addition, for demonstrating the superiority of OSAEDH-PPCA, several existing MFs [27], [35], [36] are also selected to process the signal.

A. EXPERIMENTAL SIGNAL FROM THE IMS

The experimental signal is acquired from the Intelligent Maintenance Systems (IMS), University of Cincinnati. The schematic diagram of the test rig is shown in Fig. 10. There are four rolling bearings in the test rig and driven by an AC motor. More detailed information of the test rig can be obtained in [46]. The rotation speed of the shaft is 2000rpm. The sampling frequency is 20000 Hz. The related parameters of the rolling bearing are given in Table 2. According to Table 2, it can be calculated that the fault frequency of outer race (f_o) is 236.4 Hz, and the fault frequency of inner race (f_i) is 296.9 Hz.

All the test data divides into three sets, and the 2nd set data is selected for the analysis. In the 2nd set data, the vibration signal is collected every 10 minutes. After continuous operation over 7 days, 984 data files can be obtained. In addition, the outer race failure of bearing No. 1 in Fig. 10 has emerged. Meanwhile, the state change of bearing No. 1 in the whole

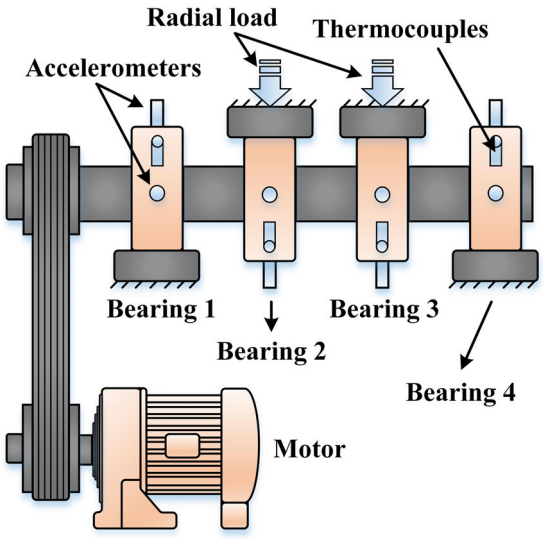

FIGURE 10. The schematic diagram of bearing fault test rig.

TABLE 2. The parameters of rolling bearing.

Related parameters	Parameter values
Bearing type	Rexnord ZA-2115
Pitch diameter	71.501 mm
Number of roller	16
Roller diameter	8.4074 mm
Contact angle	15.17°

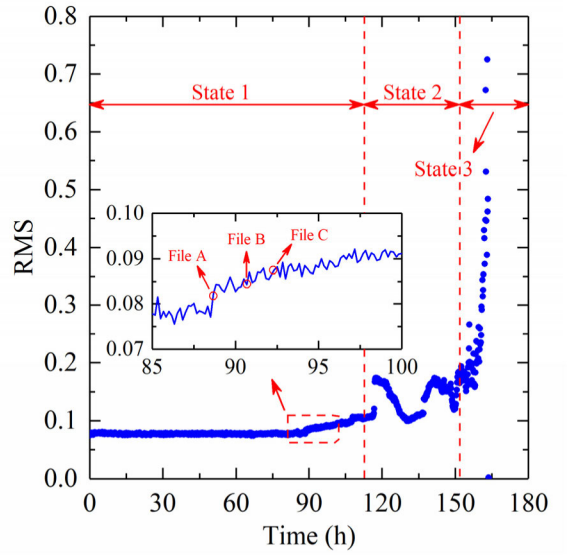

FIGURE 11. The RMS value curve of bearing No. 1.

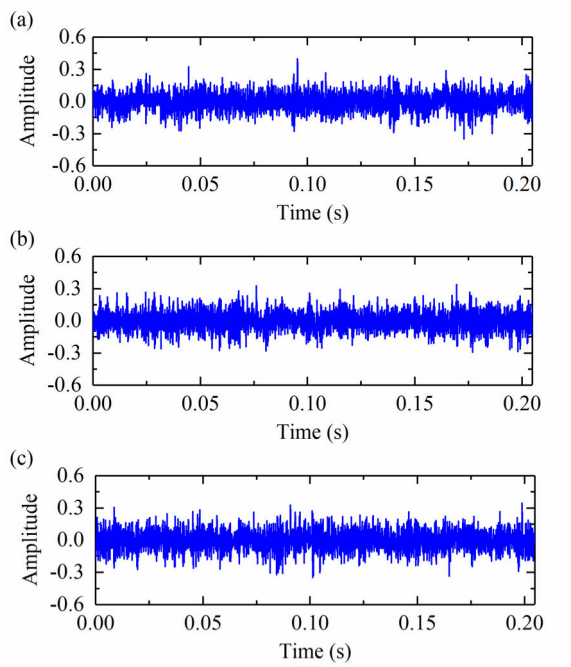

FIGURE 12. Early fault signals of bearing No. 1 in different files: (a) the time domain waveform of file A, (b) the time domain waveform of file B, (c) the time domain waveform of file C.

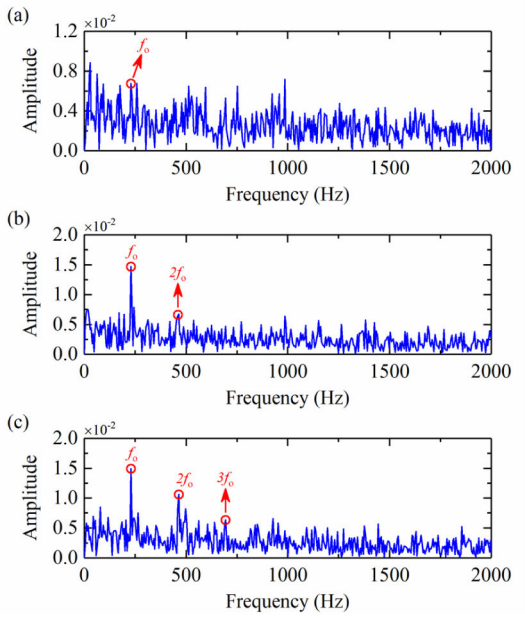

FIGURE 13. Envelope spectrums of bearing No. 1 in different files: (a) file A, (b) file B, (c) file C.

life cycle can be obtained. Fig. 11 shows the variation of RMS value about bearing No. 1 during the whole life cycle. According to the conclusions in [46], the life cycle of the bearing No. 1 can be divided into three stages (state 1, state 2, state 3). These three stages correspond to the early defect, middle defect and the last failure of the bearing No. 1. In practical application, it is very significant to detect the early fault of rolling bearings. In the early stage, three sets of data are chosen for the next analysis. The selected experimental data files (file A, B and C) are shown in Fig. 11. The time domain waveforms and envelope spectrums of the selected

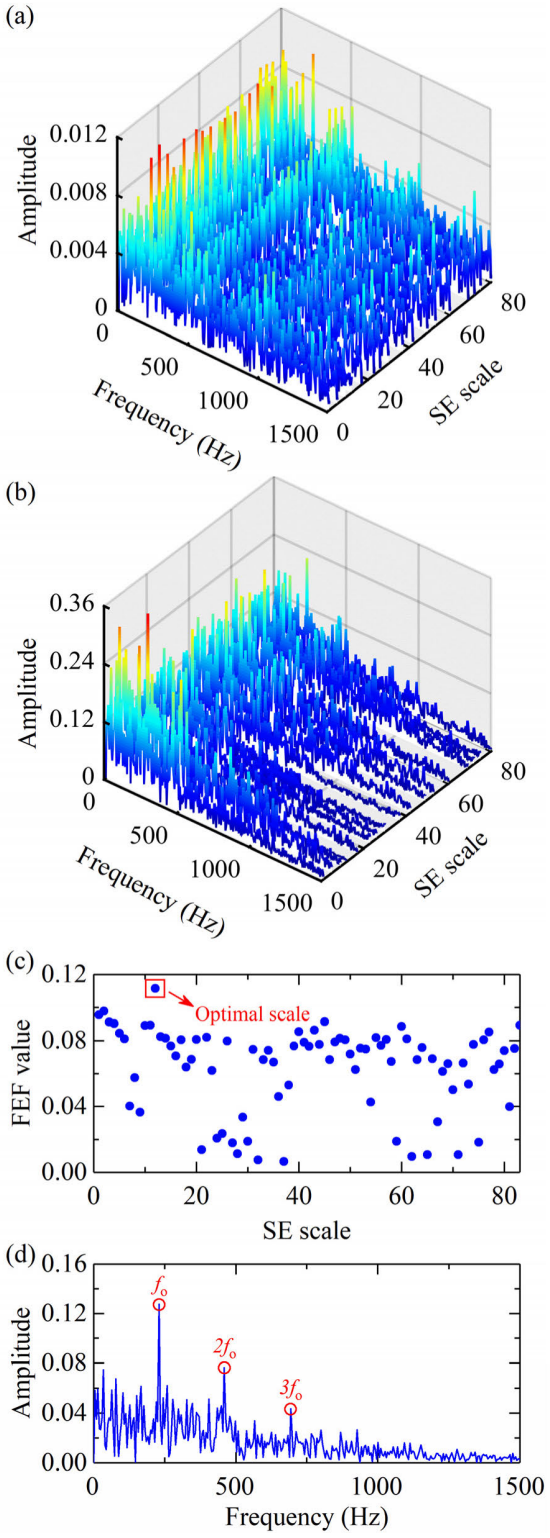

FIGURE 14. The analysis result of OSAEDH-PPCA: (a) envelope spectrums at different scales after AEDH, (b) envelope spectrums at different scales after AEDH-PPCA, (c) FEF curve of AEDH-PPCA, (d) envelope spectrum of the optimal scale.

experimental signals are shown in Figs. 12-13. By comparing the envelope spectrums of file A, B and C, the fault frequency f_o in file A is significantly more difficult to be detected.

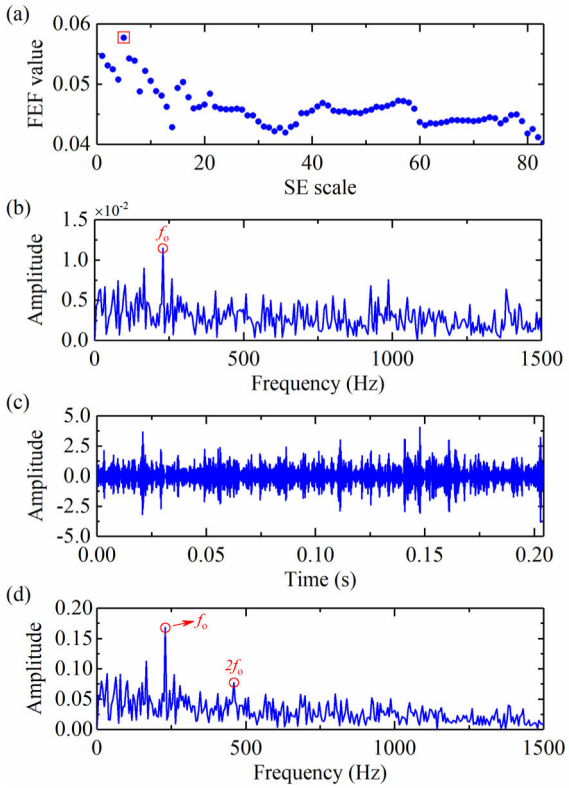

FIGURE 15. The analysis result of AMCMFH-PPCA: (a) FEF curve of AMCMFH, (b) the envelope spectrum of AMCMFH, (c) the time domain waveform of AMCMFH-PPCA, (d) the envelope spectrum of AMCMFH-PPCA.

Moreover, there are a large number of interference frequencies existing in the envelope spectrum of file A. Meanwhile, the collection time of file A is earlier than the other two files. Hence, according to above conclusions, the experimental signal of bearing No. 1 in the file A is selected to verify the effectiveness of OSAEDH-PPCA.

In order to extract the fault feature, proposed method is applied to process the experimental signal. Fig. 14 shows the filtered result of OSAEDH-PPCA. The envelope spectrums of the AEDH results at different SE scales are shown in Fig. 14(a). It can be observed that there is still some noise in the filtered results of AEDH, and that may still have effect on the accuracy of fault diagnosis. According to Fig. 14(b), the noise has been separated by PPCA effectively, and the fault features have been highlighted. Fig. 14(c) shows the FEF values of the AEDH-PPCA filtered results. When the SE scale is 12, the maximum of FEF is obtained (FEF = 0.1115). Therefore, the filtered result of AEDH-PPCA at scale 12 is used as the final output. The envelope spectrum of the final output is shown in Fig. 14(d). It can be observed that the fault frequency fo of outer race and its harmonic frequencies (2fo, 3fo) can be detected clearly. Meanwhile, compared with Fig. 13(a), the noise in the experimental signal is also significantly suppressed. It means that the early fault of

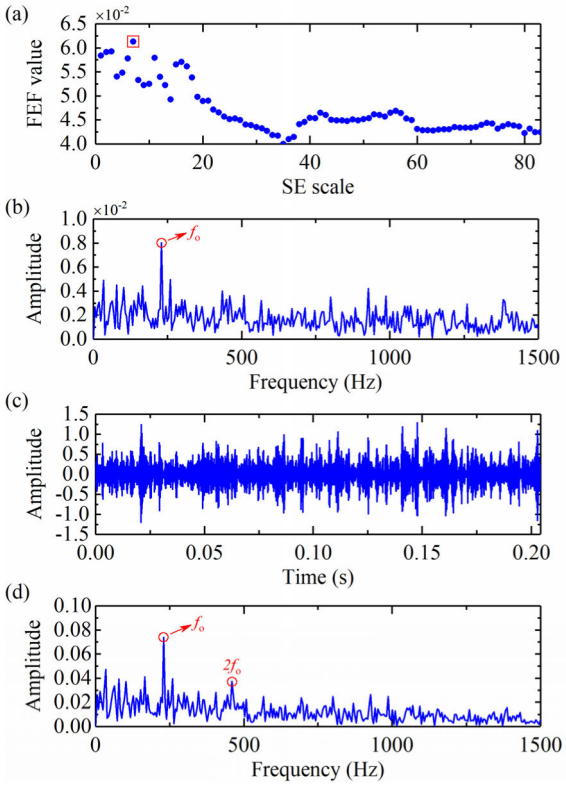

FIGURE 16. The analysis result of AMAVGH-PPCA: (a) FEF curve of AMAVGH, (b) the envelope spectrum of AMAVGH, (c) the time domain waveform of AMAVGH-PPCA, (d) the envelope spectrum of AMAVGH-PPCA.

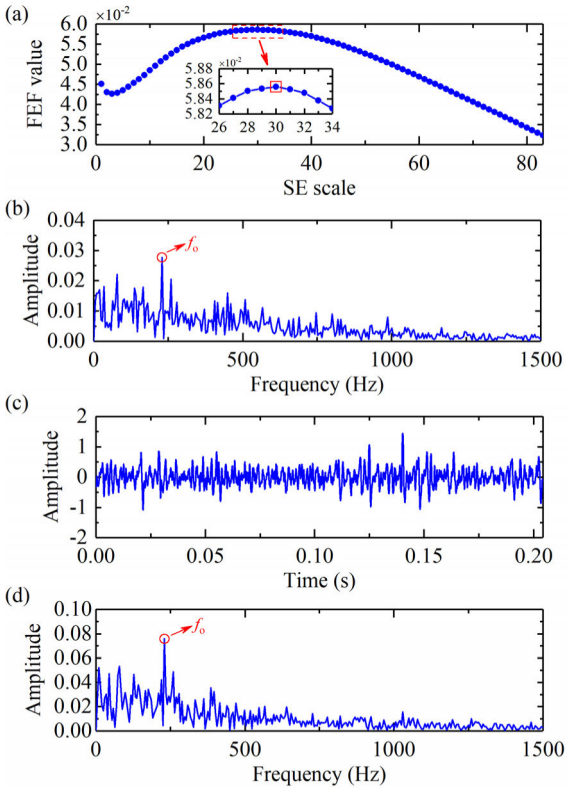

FIGURE 17. The analysis result of $AMMG_{DE}$-PPCA: (a) FEF curve of $AMMG_{DE}$, (b) the envelope spectrum of $AMMG_{DE}$, (c) the time domain waveform of $AMMG_{DE}$-PPCA, (d) the envelope spectrum of $AMMG_{DE}$-PPCA.

rolling bearing can be detected by proposed OSAEDH-PPCA effectively.

For comparison, several existing MFs are introduced to process the experimental signal. In Yan's adaptive multiscale CMFH transform (AMCMFH) [27], CMFH operator was employed to construct a multiscale morphological filter, and the FEF value was also selected to determine the optimal scale. Similarly, replacing the CMFH operator in Yan's method with the AVGH operator can constitute a new MF, namely adaptive multiscale AVGH transform (AMAVGH). The researchers in [36] adopted the MG operator and DIF operator to propose two averaged multiscale MFs, namely averaged multiscale MG filter ($AMMG_{DE}$) and averaged multiscale DIF filter ($AMMG_{CO}$). Meanwhile, in Li's method, the characteristic frequency intensity coefficient (CFIC) was employed to selected the final output. Yu *et al.* [35] proposed an average combination difference morphological filter (ACDIF) to extract the fault features in the vibration signal. In Yu's method, the Teager energy kurtosis (TEK) was applied to decide the optimal scale. According to the studies of above scholars, FEF, CFIC and TEK have been proved to be able to optimize the SE scale of MF. Therefore, in the following discussions, we only use FEF to optimize the SE scale of other existing MFs for the conformity. In view of proposed method uses PPCA to process the filtered results of AEDH while other existing MFs do not. For the fairness of comparisons, PPCA is also introduced into other existing MFs to further process their filtered results.

The filtered results of existing MFs (AMCMFM, AMAVGH, $AMMG_{DE}$, $AMMG_{CO}$ and ACDIF) and MFs-PPCA (AMCMFH-PPCA, AMAVGH-PPCA, $AMMG_{DE}$-PPCA, $AMMG_{CO}$-PPCA and ACDIF-PPCA) are shown in Figs. 15-19. In the analysis result of AMCMFH (Fig. 15(a)), when the SE scale is 5, the maximum FEF value can be obtained (FEF = 0.0577). Meanwhile, the analysis result of AMAVGH (Fig. 16(a)) shows the maximum FEF value can be obtained at scale 7 (FEF = 0.0613). It can be observed in the envelope spectrums of AMCMFH (Fig. 15(b)) and AMAVGH (Fig. 16(b)) that the fault frequency f_o can be detected. Furthermore, after processed by PPCA, the noise in the envelope spectrum has been suppressed effectively. However, compared with Fig. 14, the harmonics of characteristic frequency can be detected reluctantly ($2f_o$), and more harmonic frequencies cannot be detected. According to the discussions in Section 3, the feature extraction capability of AEDH is superior to CMFH and AVGH. In view of the insufficient feature extraction capability of the MFs based on CMFH and AVGH, it is difficult to detect more harmonics of fault frequency even if PPCA is further applied for noise reduction.

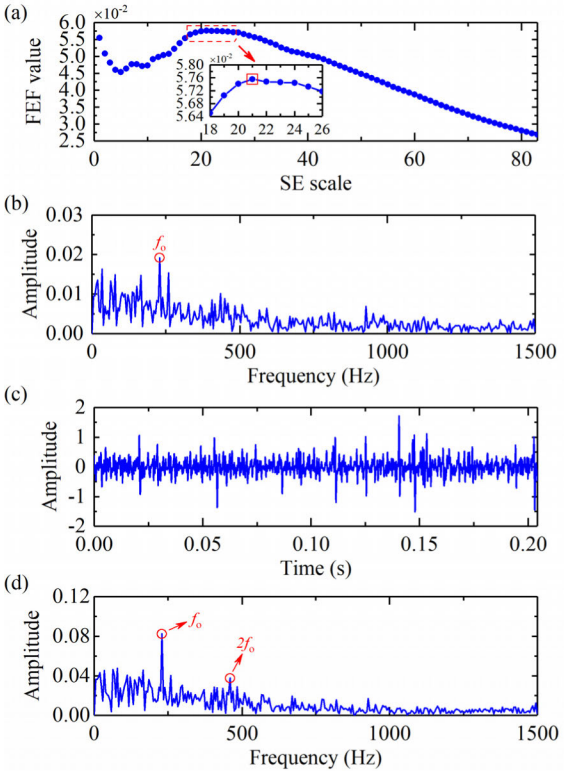

FIGURE 18. The analysis result of AMMG$_{CO}$-PPCA: (a) FEF curve of AMMG$_{CO}$, (b) the envelope spectrum of AMMG$_{CO}$, (c) the time domain waveform of AMMG$_{CO}$-PPCA, (d) the envelope spectrum of AMMG$_{CO}$-PPCA.

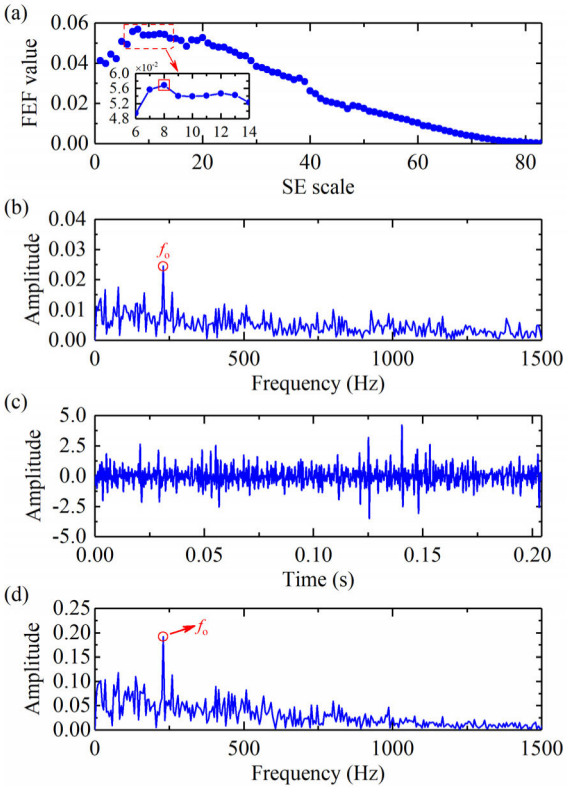

FIGURE 19. The analysis result of ACDIF-PPCA: (a) FEF curve of ACDIF, (b) the envelope spectrum of ACDIF, (c) the time domain waveform of ACDIF-PPCA, (d) the envelope spectrum of ACDIF-PPCA.

In Figs. 17-18, when the SE scale is 30 and 21 respectively, AMMG$_{DE}$ (FEF = 0.0586) and AMMG$_{CO}$ (FEF = 0.0576) obtain the maximum FEF values. Moreover, it can be indicated that AMMG$_{DE}$ and AMMG$_{CO}$ can suppress the noise in original signal effectively. Unfortunately, because many details of fault information are filtered out, the harmonic frequencies of f_o cannot be detected in the envelope spectrum. Furthermore, it can be observed in Fig. 17(d) and Fig. 18(d) that the introduction of PPCA has little effect on the final results. Since a lot of feature information in the previous results have been filtered, the post-processing can only remove the noise again. The loss of a large amount of fault feature information will make it difficult to further study the fault mechanism, and increases the difficulties of fault diagnosis. In Fig. 19, similar to AMMG$_{DE}$ and AMMG$_{CO}$, although ACDIF at the optimal SE scale (scale 8, FEF = 0.0569) shows excellent noise suppression capability, the harmonic frequencies of the fault frequency f_o cannot be detected either. In addition, PPCA also has little effect on the final result due to the loss of fault feature information in ACDIF result. To sum up, the analysis results of Figs. 15-19 show that it is difficult for existing MFs to effectively extract fault information even if PPCA is employed as a post-processing tool. Therefore, compared with existing MFs, the proposed OSAEDH-PPCA can accurately detect the early defect of rolling bearing.

TABLE 3. The parameters of rolling bearing.

Related parameters	Parameter values
Bearing type	SKF NU 1030
Outside diameter	225 mm
Inside diameter	150 mm
Pitch diameter	187.5 mm
Number of roller	24
Roller diameter	18 mm
Contact angle	0°

B. ENGINEERING APPLICATION IN WIND TURBINE

As a kind of clean energy, wind energy has been paid more and more attention to the power generation industry of various countries in the world. At the same time, wind energy resources are widely distributed in most countries and regions, which greatly facilitates the widespread application of wind power generation technology. However, since the wind turbines often work in extreme environments, the transmission system will be prone to failure. Serious failures of key components such as bearings in the transmission system may cause the shutdown of wind turbine and huge economic losses. Hence, it is significant to extract the feature signal in the early stage of failure for the fault diagnosis of

FIGURE 20. Vibration signal collection of the abnormal bearing.

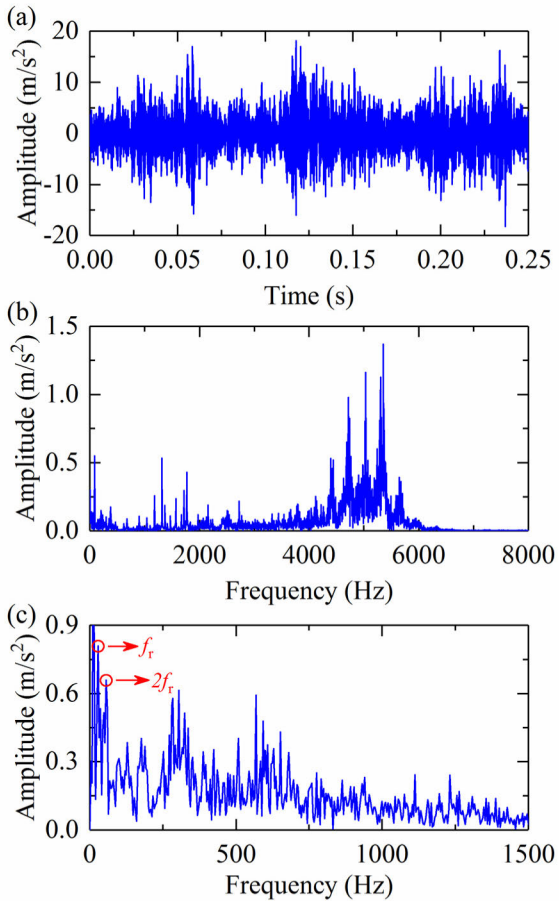

FIGURE 21. Test signal of abnormal bearing: (a) time domain waveform, (b) FFT spectrum, (c) envelope spectrum.

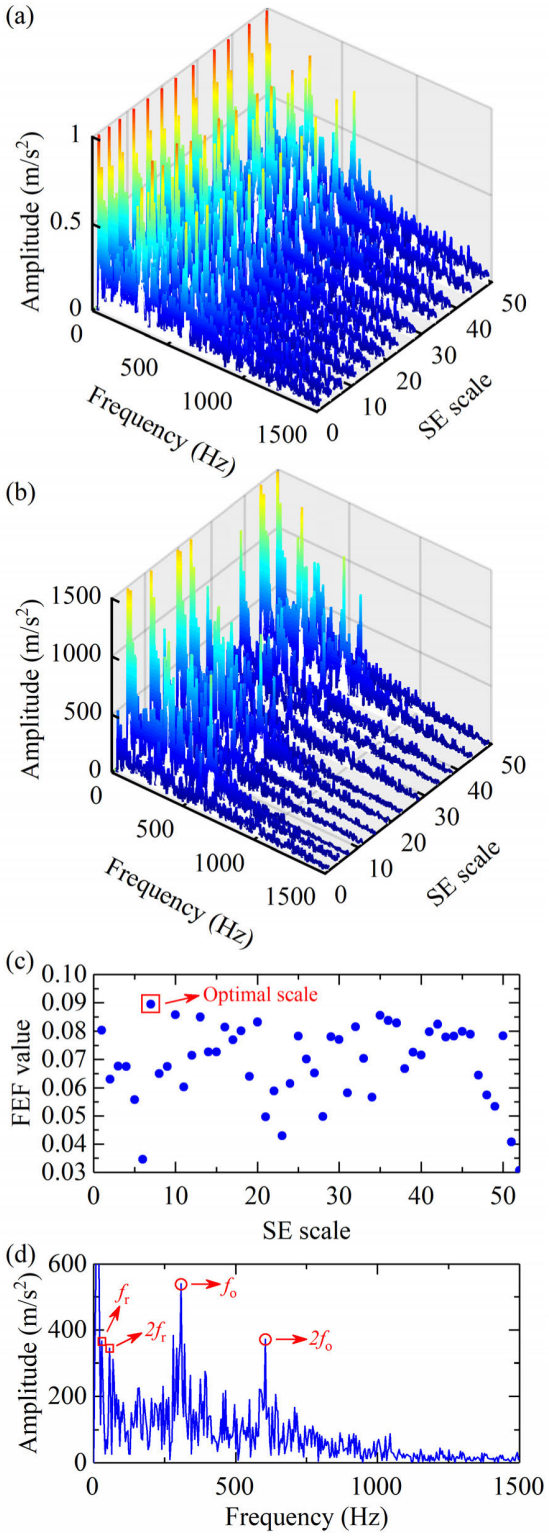

FIGURE 22. The filtered result of OSAEDH-PPCA: (a) envelope spectrums at different scales after AEDH, (b) envelope spectrums at different scales after AEDH-PPCA, (c) FEF curve of AEDH-PPCA, (d) envelope spectrum of the optimal scale.

wind turbines. In the following, the effectiveness of proposed OSAEDH-PPCA is validated by employing the vibration signal collected from the wind farm.

After monitoring the No. 16 wind turbine (the rated power is 1.5 MW) in the Tuoshan Wind Farm, it can be found that the abnormal vibration of the generator

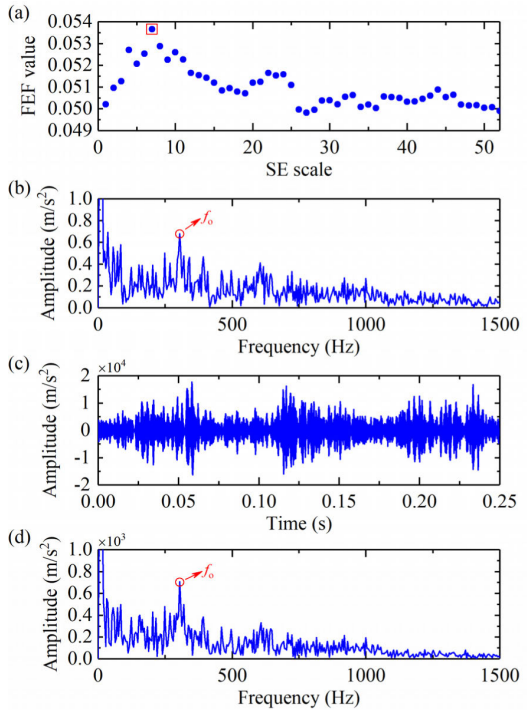

FIGURE 23. The filtered result of AMCMFH-PPCA: (a) FEF curve of AMCMFH, (b) the envelope spectrum of AMCMFH, (c) the time domain waveform of AMCMFH-PPCA, (d) the envelope spectrum of AMCMFH-PPCA.

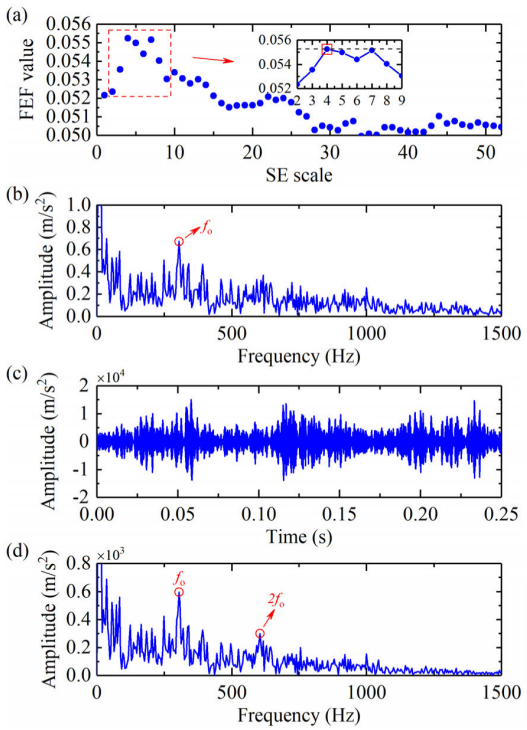

FIGURE 24. The filtered result of AMAVGH-PPCA: (a) FEF curve of AMAVGH, (b) the envelope spectrum of AMAVGH, (c) the time domain waveform of AMAVGH-PPCA, (d) the envelope spectrum of AMAVGH-PPCA.

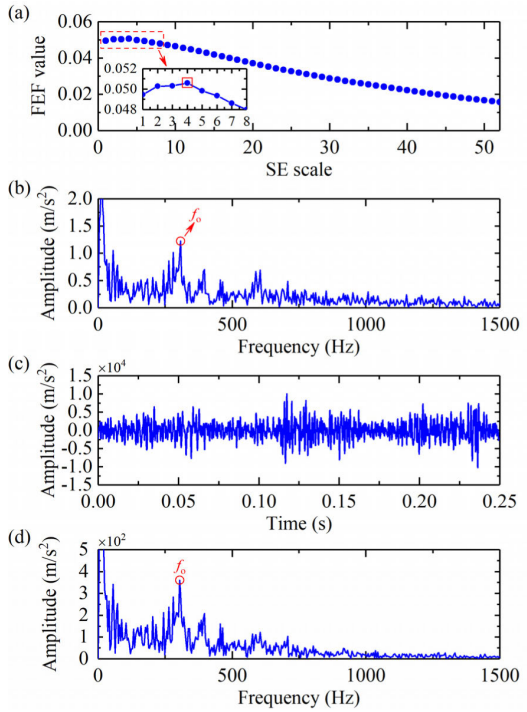

FIGURE 25. The filtered result of AMMG$_{DE}$-PPCA: (a) FEF curve of AMMG$_{DE}$, (b) the envelope spectrum of AMMG$_{DE}$, (c) the time domain waveform of AMMG$_{DE}$-PPCA, (d) the envelope spectrum of AMMG$_{DE}$-PPCA.

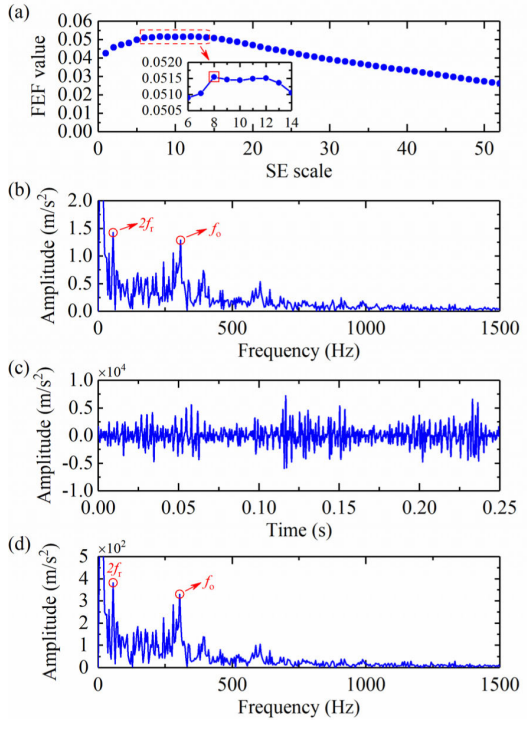

FIGURE 26. The filtered result of AMMG$_{CO}$-PPCA: (a) FEF curve of AMMG$_{CO}$, (b) the envelope spectrum of AMMG$_{CO}$, (c) the time domain waveform of AMMG$_{CO}$-PPCA, (d) the envelope spectrum of AMMG$_{CO}$-PPCA.

front bearing appeared. The type of the abnormal bearing is NU1030, and its related parameters are shown in Table 3.

The rotation speed of the generator is 1680rpm (the rotation frequency $f_r = 28$ Hz). It can be calculated that the fault frequency of the outer race in the abnormal bearing

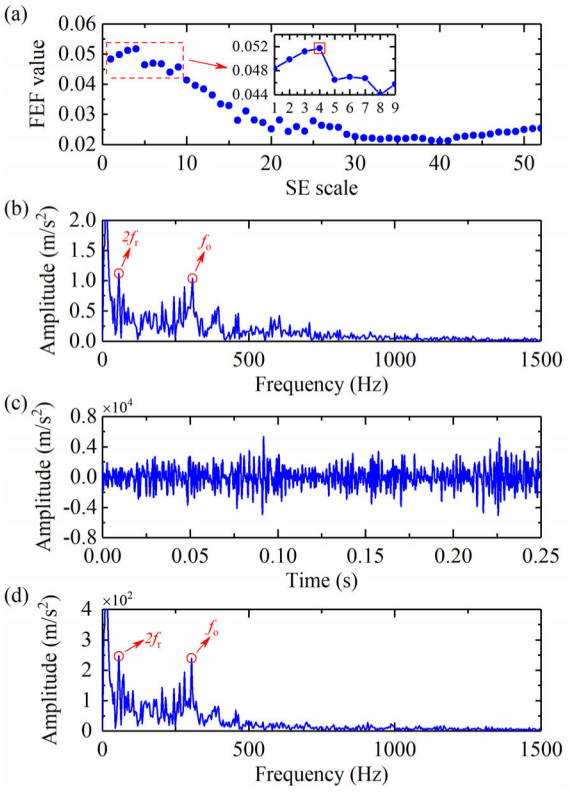

FIGURE 27. The filtered result of ACDIF-PPCA: (a) FEF curve of ACDIF, (b) the envelope spectrum of ACDIF, (c) the time domain waveform of ACDIF-PPCA, (d) the envelope spectrum of ACDIF-PPCA.

f_o = 303.74 Hz, and the fault frequency of the inner race in the abnormal bearing f_i = 368.26 Hz. The test vibration signal can be obtained by the data collection of abnormal bearing. The data collection site in the wind turbine is shown in Fig. 20. The sampling frequency is 16384 Hz. The time domain waveform, FFT spectrum, and envelope spectrum of the collected test signal are shown in Fig. 21. In the envelope spectrum, it can be observed that only the rotation frequency and its harmonic frequency (f_r, $2f_r$) can be clearly detected.

In order to investigate the cause of bearing anomaly, the proposed OSAEDH-PPCA is employed to process the test signal. Fig. 22 shows the analysis result of proposed method. It can be observed that scale 7 obtains the maximum FEF value (FEF = 0.0894). Thus, the filtered result of AEDH-PPCA at scale 7 is used as the final output. In Fig. 22(d), It can be obviously observed that two peaks can be detected in the envelope spectrum, and the frequencies corresponding to these two peaks are 304 Hz and 608 Hz. Those two frequencies are very close to the fault frequency of the outer race in the abnormal bearing (f_o = 303.74 Hz and $2f_o$ = 607.49 Hz). Hence, the analysis result indicates that the outer race defect occurs in the generator front bearing. The conclusion can also explain why the abnormal vibration of the generator front bearing occurs. Then, in order to avoid economic losses, it is necessary to continue collecting the vibration data of abnormal bearing and determine the appropriate maintenance time.

Figs. 23-27 show the analysis results of existing MFs (AMCMFM, AMAVGH, $AMMG_{DE}$, $AMMG_{CO}$ and ACDIF) and MFs-PPCA (AMCMFH-PPCA, AMAVGH-PPCA, $AMMG_{DE}$-PPCA, $AMMG_{CO}$-PPCA and ACDIF-PPCA), respectively. The maximum FEF values of AMCMFM (scale 7, FEF = 0.0537), AMAVGH (scale 4, FEF = 0.0552), $AMMG_{DE}$ (scale 4, FEF = 0.0505), $AMMG_{CO}$ (scale 8, FEF = 0.0515) and ACDIF (scale 4, FEF = 0.0517) can be obtained in Fig. 23(a), Fig. 24(a), Fig. 25(a), Fig. 26(a) and Fig. 27(a). In Figs 23-24, the fault frequency and its harmonics cannot be detected clearly in the envelope spectrums of AMCMFH-PPCA and AMAVGH-PPCA. In other words, for the diagnosis in this test, the accuracy of AMCMFH-PPCA and AMAVGH-PPCA is relatively insufficient. The results of $AMMG_{DE}$-PPCA, $AMMG_{CO}$-PPCA, and ACDIF-PPCA (Figs. 25-27) show that three MFs have certain noise suppression capability. Unfortunately, a lot of frequencies information related to the fault is also filtered out. Meanwhile, the final results of PPCA post-processing show that there is no obvious difference compared to before. Moreover, it can be observed that the peaks of interference frequencies around the fault frequency are still prominent. Those peaks may mislead the diagnosis of abnormal bearing. According to the comparison results, it can be found that the proposed OSAEDH-PPCA is able to detect bearing fault in the early state more effectively.

VI. CONCLUSION

In this paper, a new OSAEDH-PPCA method is presented for detecting the defect of rolling bearings from vibration signals. Firstly, a new morphological top-hat operator AEDH is proposed based on the morphological erosion and dilation operators. Simulation analyses demonstrate the filter characteristics of AEDH operator and verify that the fault feature extraction capability of AEDH operator is superior to the existing morphological top-hat operators. Then, considering that the noise may have effect on the filter property of AEDH operator, PPCA is introduced to construct OSAEDH-PPCA for highlighting the fault feature information further. In order to verify the availability of proposed method, OSAEDH-PPCA is used to process the experimental signals acquired from the test rig and practical engineering. The results of experiment and engineering application show that the early defect of rolling bearing can be detected by OSAEDH-PPCA successfully. Comparison results indicate that the proposed OSAEDH-PPCA is superior to existing MFs in the fault diagnosis of rolling bearing. In the future works, proposed method will be further applied in more working conditions, such as the gear faults in the planetary gearbox of a wind turbine.

REFERENCES

[1] H. Shi, L. Guo, S. Tan, and X. Bai, "Rolling bearing initial fault detection using long short-term memory recurrent network," *IEEE Access*, vol. 7, pp. 171559–171569, 2019, doi: 10.1109/ACCESS.2019.2954091.

[2] R. B. Randall and J. Antoni, "Rolling element bearing diagnostics—A tutorial," *Mech. Syst. Signal Process.*, vol. 25, no. 2, pp. 485–520, Feb. 2011, doi: 10.1016/j.ymssp.2010.07.017.
[3] Z. Feng, M. Liang, and F. Chu, "Recent advances in time–frequency analysis methods for machinery fault diagnosis: A review with application examples," *Mech. Syst. Signal Process.*, vol. 38, no. 1, pp. 165–205, Jul. 2013, doi: 10.1016/j.ymssp.2013.01.017.
[4] Z. Dong, X. Sun, F. Xu, and W. Liu, "A low-rank and sparse decomposition-based method of improving the accuracy of sub-pixel grayscale centroid extraction for spot images," *IEEE Sensors J.*, vol. 20, no. 11, pp. 5845–5854, Jun. 2020, doi: 10.1109/JSEN.2020.2974725.
[5] R. Yan, R. X. Gao, and X. Chen, "Wavelets for fault diagnosis of rotary machines: A review with applications," *Signal Process.*, vol. 96, pp. 1–15, Mar. 2014, doi: 10.1016/j.sigpro.2013.04.015.
[6] J. Antoni and R. B. Randall, "The spectral kurtosis: Application to the vibratory surveillance and diagnostics of rotating machines," *Mech. Syst. Signal Process.*, vol. 20, no. 2, pp. 308–331, Feb. 2006, doi: 10.1016/j.ymssp.2004.09.002.
[7] D. P. Mandic, N. U. Rehman, Z. Wu, and N. E. Huang, "Empirical mode decomposition-based time-frequency analysis of multivariate signals: The power of adaptive data analysis," *IEEE Signal Process. Mag.*, vol. 30, no. 6, pp. 74–86, Nov. 2013, doi: 10.1109/MSP.2013.2267931.
[8] K. Dragomiretskiy and D. Zosso, "Variational mode decomposition," *IEEE Trans. Signal Process.*, vol. 62, no. 3, pp. 531–544, Feb. 2014, doi: 10.1109/TSP.2013.2288675.
[9] W. Sun, G. An Yang, Q. Chen, A. Palazoglu, and K. Feng, "Fault diagnosis of rolling bearing based on wavelet transform and envelope spectrum correlation," *J. Vibrat. Control*, vol. 19, no. 6, pp. 924–941, Apr. 2013, doi: 10.1177/1077546311435348.
[10] B. Chen, Z. Zhang, Y. Zi, Z. He, and C. Sun, "Detecting of transient vibration signatures using an improved fast spatial–spectral ensemble kurtosis kurtogram and its applications to mechanical signature analysis of short duration data from rotating machinery," *Mech. Syst. Signal Process.*, vol. 40, no. 1, pp. 1–37, Oct. 2013, doi: 10.1016/j.ymssp.2013.03.021.
[11] Y. Lei, J. Lin, Z. He, and M. J. Zuo, "A review on empirical mode decomposition in fault diagnosis of rotating machinery," *Mech. Syst. Signal Process.*, vol. 35, nos. 1–2, pp. 108–126, Feb. 2013, doi: 10.1016/j.ymssp.2012.09.015.
[12] S. Zhang, Y. Wang, S. He, and Z. Jiang, "Bearing fault diagnosis based on variational mode decomposition and total variation denoising," *Meas. Sci. Technol.*, vol. 27, no. 7, p. 75101, 2016, doi: 10.1088/0957-0233/27/7/075101.
[13] J. Ma, J. Wu, and X. Wang, "Incipient fault feature extraction of rolling bearings based on the MVMD and Teager energy operator," *ISA Trans.*, vol. 80, pp. 297–311, Sep. 2018, doi: 10.1016/j.isatra.2018.05.017.
[14] P. Maragos and R. Schafer, "Morphological filters—Part I: Their set-theoretic analysis and relations to linear shift-invariant filters," *IEEE Trans. Acoust., Speech, Signal Process.*, vol. 35, no. 8, pp. 1153–1169, Aug. 1987, doi: 10.1109/TASSP.1987.1165259.
[15] P. Maragos and R. Schafer, "Morphological filters—Part II: Their relations to median, order-statistic, and stack filters," *IEEE Trans. Acoust., Speech, Signal Process.*, vol. 35, no. 8, pp. 1170–1184, Aug. 1987, doi: 10.1109/TASSP.1987.1165254.
[16] J. Serra, "Morphological filtering: An overview," *Signal Process.*, vol. 38, no. 1, pp. 3–11, 1994, doi: 10.1016/0165-1684(94)90052-3.
[17] Y. Wu, C. Shen, H. Cao, and X. Che, "Improved morphological filter based on variational mode decomposition for MEMS gyroscope de-noising," *Micromachines*, vol. 9, no. 5, p. 246, May 2018, doi: 10.3390/mi9050246.
[18] T. Gong, X. Yuan, X. Lei, Y. Yuan, and B. Zhang, "Fault detection for rolling element bearing based on repeated single-scale morphology and simplified sensitive factor algorithm," *Measurement*, vol. 127, pp. 348–355, Oct. 2018, doi: 10.1016/j.measurement.2018.05.082.
[19] Y. Dong, M. Liao, X. Zhang, and F. Wang, "Faults diagnosis of rolling element bearings based on modified morphological method," *Mech. Syst. Signal Process.*, vol. 25, no. 4, pp. 1276–1286, May 2011, doi: 10.1016/j.ymssp.2010.10.008.
[20] J. Wang, G. Xu, Q. Zhang, and L. Liang, "Application of improved morphological filter to the extraction of impulsive attenuation signals," *Mech. Syst. Signal Process.*, vol. 23, no. 1, pp. 236–245, Jan. 2009, doi: 10.1016/j.ymssp.2008.03.012.
[21] F. F. Costa, A. J. Sguarezi Filho, C. E. Capovilla, and I. R. S. Casella, "Morphological filter applied in a wireless deadbeat control scheme within the context of smart grids," *Electr. Power Syst. Res.*, vol. 107, pp. 175–182, Feb. 2014, doi: 10.1016/j.epsr.2013.09.016.
[22] A. Hu and L. Xiang, "Selection principle of mathematical morphological operators in vibration signal processing," *J. Vibrat. Control*, vol. 22, no. 14, pp. 3157–3168, Aug. 2016, doi: 10.1177/1077546314560783.
[23] B. Li, P.-L. Zhang, Z.-J. Wang, S.-S. Mi, and D.-S. Liu, "A weighted multi-scale morphological gradient filter for rolling element bearing fault detection," *ISA Trans.*, vol. 50, no. 4, pp. 599–608, Oct. 2011, doi: 10.1016/j.isatra.2011.06.003.
[24] A. S. Raj and N. Murali, "Early classification of bearing faults using morphological operators and fuzzy inference," *IEEE Trans. Ind. Electron.*, vol. 60, no. 2, pp. 567–574, Feb. 2013, doi: 10.1109/TIE.2012.2188259.
[25] Y. Li, X. Liang, and M. J. Zuo, "Diagonal slice spectrum assisted optimal scale morphological filter for rolling element bearing fault diagnosis," *Mech. Syst. Signal Process.*, vol. 85, pp. 146–161, Feb. 2017, doi: 10.1016/j.ymssp.2016.08.019.
[26] L. Zhang, J. Xu, J. Yang, D. Yang, and D. Wang, "Multiscale morphology analysis and its application to fault diagnosis," *Mech. Syst. Signal Process.*, vol. 22, no. 3, pp. 597–610, Apr. 2008, doi: 10.1016/j.ymssp.2007.09.010.
[27] X. Yan, M. Jia, W. Zhang, and L. Zhu, "Fault diagnosis of rolling element bearing using a new optimal scale morphology analysis method," *ISA Trans.*, vol. 73, pp. 165–180, Feb. 2018, doi: 10.1016/j.isatra.2018.01.004.
[28] X. Yan and M. Jia, "Application of CSA-VMD and optimal scale morphological slice bispectrum in enhancing outer race fault detection of rolling element bearings," *Mech. Syst. Signal Process.*, vol. 122, pp. 56–86, May 2019, doi: 10.1016/j.ymssp.2018.12.022.
[29] Q. Chen, Z. Chen, W. Sun, G. Yang, A. Palazoglu, and Z. Ren, "A new structuring element for multi-scale morphology analysis and its application in rolling element bearing fault diagnosis," *J. Vibrat. Control*, vol. 21, no. 4, pp. 765–789, Mar. 2015, doi: 10.1177/1077546313486163.
[30] Y. Li, X. Liang, and M. J. Zuo, "A new strategy of using a time-varying structure element for mathematical morphological filtering," *Measurement*, vol. 106, pp. 53–65, Aug. 2017, doi: 10.1016/j.measurement.2017.04.032.
[31] Z. Hu, C. Wang, J. Zhu, X. Liu, and F. Kong, "Bearing fault diagnosis based on an improved morphological filter," *Measurement*, vol. 80, pp. 163–178, Feb. 2016, doi: 10.1016/j.measurement.2015.11.028.
[32] L. Cui, J. Wang, and J. Ma, "Early fault detection method for rolling bearing based on multiscale morphological filtering of information-entropy threshold," *J. Mech. Sci. Technol.*, vol. 33, no. 4, pp. 1513–1522, Apr. 2019, doi: 10.1007/s12206-019-0303-4.
[33] A. Hu and L. Xiang, "An optimal selection method for morphological filter's parameters and its application in bearing fault diagnosis," *J. Mech. Sci. Technol.*, vol. 30, no. 3, pp. 1055–1063, Mar. 2016, doi: 10.1007/s12206-016-0208-4.
[34] J. Yu, T. Hu, and H. Liu, "A new morphological filter for fault feature extraction of vibration signals," *IEEE Access*, vol. 7, pp. 53743–53753, 2019, doi: 10.1109/ACCESS.2019.2912898.
[35] J. Lv and J. Yu, "Average combination difference morphological filters for fault feature extraction of bearing," *Mech. Syst. Signal Process.*, vol. 100, pp. 827–845, Feb. 2018, doi: 10.1016/j.ymssp.2017.08.020.
[36] B. Li, P.-L. Zhang, Z.-J. Wang, S.-S. Mi, and Y.-T. Zhang, "Gear fault detection using multi-scale morphological filters," *Measurement*, vol. 44, no. 10, pp. 2078–2089, Dec. 2011, doi: 10.1016/j.measurement.2011.08.010.
[37] Y. Li, M. J. Zuo, J. Lin, and J. Liu, "Fault detection method for railway wheel flat using an adaptive multiscale morphological filter," *Mech. Syst. Signal Process.*, vol. 84, pp. 642–658, Feb. 2017, doi: 10.1016/j.ymssp.2016.07.009.
[38] M. E. Tipping and C. M. Bishop, "Probabilistic principal component analysis," *J. Roy. Stat. Soc. Ser. B, Stat. Methodol.*, vol. 61, no. 3, pp. 611–622, Aug. 1999, doi: 10.1111/1467-9868.00196.
[39] D. Kim and I.-B. Lee, "Process monitoring based on probabilistic PCA," *Chemometrics Intell. Lab. Syst.*, vol. 67, no. 2, pp. 109–123, 2003, doi: 10.1016/S0169-7439(03)00063-7.
[40] C. M. Bishop and M. E. Tipping, "A hierarchical latent variable model for data visualization," *IEEE Trans. Pattern Anal. Mach. Intell.*, vol. 20, no. 3, pp. 281–293, Mar. 1998, doi: 10.1109/34.667885.
[41] N. G. Nikolaou and I. A. Antoniadis, "Application of morphological operators as envelope extractors for impulsive-type periodic signals," *Mech. Syst. Signal Process.*, vol. 17, no. 6, pp. 1147–1162, Nov. 2003, doi: 10.1006/mssp.2002.1576.
[42] X. Zhang, Q. Miao, H. Zhang, and L. Wang, "A parameter-adaptive VMD method based on grasshopper optimization algorithm to analyze vibration signals from rotating machinery," *Mech. Syst. Signal Process.*, vol. 108, pp. 58–72, Aug. 2018, doi: 10.1016/j.ymssp.2017.11.029.

[43] X. Yan, M. Jia, and L. Xiang, "Compound fault diagnosis of rotating machinery based on OVMD and a 1.5-dimension envelope spectrum," *Meas. Sci. Technol.*, vol. 27, no. 7, pp. 75002–75017, 2016, doi: 10.1088/0957-0233/27/7/075002.
[44] R. Sharifi and R. Langari, "Nonlinear sensor fault diagnosis using mixture of probabilistic PCA models," *Mech. Syst. Signal Process.*, vol. 85, pp. 638–650, Feb. 2017, doi: 10.1016/j.ymssp.2016.08.028.
[45] R. Golafshan and K. Yuce Sanliturk, "SVD and hankel matrix based de-noising approach for ball bearing fault detection and its assessment using artificial faults," *Mech. Syst. Signal Process.*, vols. 70–71, pp. 36–50, Mar. 2016, doi: 10.1016/j.ymssp.2015.08.012.
[46] H. Qiu, J. Lee, J. Lin, and G. Yu, "Wavelet filter-based weak signature detection method and its application on rolling element bearing prognostics," *J. Sound Vibrat.*, vol. 289, nos. 4–5, pp. 1066–1090, Feb. 2006, doi: 10.1016/j.jsv.2005.03.007.

SIYU ZHAO was born in 1993. He is currently pursuing the Ph.D. degree with the School of Mechanical Engineering, Shenyang University of Technology, China. His current interests include signal processing, intelligent fault diagnosis, and fault detection of wind turbine.

CHANGZHENG CHEN was born in 1964. He is currently a Professor and a Ph.D. Supervisor with the School of Mechanical Engineering, Shenyang University of Technology, China. His current research interests include vibration, noise, and fault diagnosis.

YUANQING LUO was born in 1990. He is currently pursuing the Ph.D. degree with the School of Mechanical Engineering, Shenyang University of Technology, China. His current research interests include the wind turbine condition monitoring and fault diagnosis.